ELSEVIER

Journal of Process Control 10 (2000) 177–184

JOURNAL OF PROCESS CONTROL

www.elsevier.com/locate/jprocont

Order reduction for nonlinear dynamic models of distributed reacting systems

S.Y. Shvartsman [a], C. Theodoropoulos [a,*], R. Rico-Martínez [b], I.G. Kevrekidis [a], E.S. Titi [c], T.J. Mountziaris [d]

[a] *Department of Chemical Engineering, Princeton University, Princeton NJ, 08544-5263, USA*
[b] *Departmento de Ingeniería Química, Instituto Tecnológico de Celaya, Gto, Mexico and Fritz-Haber-Institut der Max-Planck-Gesellschaft, Berlin, Germany*
[c] *Departments of Mathematics and of Mechanical and Aerospace Engineering, University of California, Irvine, CA, USA*
[d] *Department of Chemical Engineering, State University of New York at Buffalo, New York, USA*

Abstract

Detailed first-principles models of transport and reaction (based on partial differential equations) lead, after discretization, to dynamical systems of very high order. Systematic methodologies for model order reduction are vital in exploiting such fundamental models in the analysis, design and real-time control of distributed reacting systems. We briefly review some approaches to model order reduction we have successfully used in recent years, and illustrate their capabilities through (a) the design of an observer and stabilizing controller of a reaction-diffusion problem and (b) two-dimensional simulations of the transient behavior of a horizontal MOVPE reactor. © 2000 IFAC. Published by Elsevier Science Ltd. All rights reserved.

Keywords: Distributed systems; Model reduction; Proper orthogonal decomposition; Estimation; Control; MOVPE

1. Introduction

A (nonlinear) vectorfield constitutes the starting point for the analysis of the dynamic behavior of an open loop system and its dependence on operating parameters. It also constitutes the starting point for controller design and evaluation of closed-loop performance. Three-dimensional, time dependent partial differential equations (PDEs) employed for the modeling of reaction-transport processes lead, through accurate, resolved discretizations to models with predictive capabilities; these models, however, contain $O(10^4)$ (and often many more) degrees of freedom. While current computational hardware and software allow for the routine simulation of such system sizes, nonlinear dynamic analysis and controller design can not (and probably should not) be based on such full scale models.

It should be noted that truncation of the PDE discretization is, in itself, a model order reduction from infinite-dimensional dynamical systems to finite (albeit large) ones; the study of such truncations and their performance in controller design has been studied extensively by Balas (e.g. [1,2]) and others. In some cases reduced order models are formulated on the basis of extensive knowledge about the dynamic behavior of the system based on many years of modeling and experimentation; examples of using such models for dynamic analysis and design of controllers for distillation columns and packed bed reactors can be found in the series of papers by F. Doyle et al. (e.g. [3]).

We are interested in systematic methodologies for reducing large vectorfields, obtained through PDE discretizations, to "small", accurate, nonlinear dynamic models; obviously these reduced models will be predictive in a more narrow region of phase and parameter space than the full model. They will, on the other hand, be better conditioned and more amenable to real-time simulation and integration in control algorithms. Furthermore, if the operating regime changes, the reduction procedures can be used again to provide new reduced models, adapted to the new region of phase and parameter space. Two methodologies, partly motivated by analysis of dissipative PDEs, are beginning to enjoy extensive use in control applications. The first is the so-called method of empirical orthogonal eigenfunctions (EOFs), also termed Proper Orthogonal Decomposition (POD) and Karhunen–Loève expansion (KL). Statistical analysis of extensive simulation databases leads

* Corresponding author. Tel.: +1-609-258-2977; fax: +1-609-258-0211.
E-mail address: kostas@arnold.princeton.edu (C. Theodoropoulos).

PII: S0959-1524(99)00029-3

(through, essentially, Principal Component Analysis) to global basis functions that are then used in a Galerkin weighted residual projection of the model PDEs (see the monograph [4] for a recent review and [5–9] for a couple of representative control applications). The second, the so called Inertial Manifold and Approximate Inertial Manifold (AIM) approach [10], can be thought of as an infinite-dimensional extension of singular perturbation methods based on the separation of time scales in finite sets of ordinary differential equations (ODEs) (e.g. [11]). Center Manifold Theory provides such reductions for nonlinear dynamical systems close to specific, low-codimension bifurcation points [7,12]. Examples of the application of AIM-based reduction techniques to controller design can be found in [9,13–17].

PODs have been especially successful in formulating low-order dynamical systems in complex-geometry problems, where no simple global basis function sets are available for (pseudo)spectral discretizations (e.g. [6,18]). They can also be combined with separation of time scales methods built on top of a (linear, "flat") POD–Galerkin reduction [5,19]. Even without an explicit hierarchy of time scales, it is our experience [20,21] that slaving can be quite effective in further reducing "flat" POD–Galerkin truncations to "nonlinear-POD–Galerkin" ones, in analogy to nonlinear Galerkin methods (implementations of Approximate Inertial Manifolds in conventional spectral discretizations, ([22–24]). Remarkably, black box models, e.g. Artificial Neural Network (ANN)-based architectures, can be quite efficient in "detecting" such slaving functions (i.e. nonlinear correlations between state variables in POD-space) and in yielding vectorfields that are simply faster to evaluate [5,20].

In this contribution we illustrate the effectiveness of POD-based model reduction in the design of low-dimensional observers and controllers for a particular, one-dimensional reaction-diffusion problem; we also demonstrate the combination of POD with further, black-box based slaving techniques. We conclude with an example of POD-based reduction for a 2-D complex-geometry microelectronics fabrication reactor (a horizontal MOVPE reactor with differentially heated lower wall).

2. Examples

2.1. A nonlinear reaction–diffusion system

Consider the one-dimensional (in space) reaction diffusion system with no-flux boundary conditions which we have used as an illustrative example in previous work [8,9]

$$\frac{\partial v}{\partial t} = \frac{\partial^2 v}{\partial z^2} + f(v, w) + u(t)q(z) \tag{1}$$

$$\frac{\partial w}{\partial t} = \delta \frac{\partial^2 w}{\partial z^2} + g(v, w) \tag{2}$$

$$v_z|_{0,L} = w_z|_{0,L} = 0. \tag{3}$$

Briefly here, v is the "activator", w the "inhibitor", L the length of the one-dimensional domain, $f(v, w) \equiv v - v^3 - w$, $g(v, w) \equiv \varepsilon(v - p_1 w - p_0)$, $u(t)$ is an input (it will later become our control action) and $q(z)$ the shape of the (slightly ad hoc) actuator influence function [see Fig. 4(b)]. The open loop system ($u(t) = 0$) is known, for $L = 20$, $\delta = 4$ and $p_1 = 2$, $p_0 = -0.03$ to exhibit, in a one-parameter bifurcation diagram with respect to the parameter ε (a ratio of reaction time scales) both a supercritical Hopf bifurcation ($\varepsilon \approx 0.017$) and a turning point (saddle-node) bifurcation ($\varepsilon \approx 0.945$) of a sharp, front-like solution.

This solution, when stable, coexists with a number of other (distant in phase space) attractors. Our (pseudospectral) resolved discretization (the "full system") is a 62-dimensional Fourier-space model. Using this model we collected a database of system transient responses for ε values close to the Hopf bifurcation at various constant settings of u. This database was used to arrive at a set of empirical eigenfunctions (we chose the option of having separate eigenfunctions for each of the two concentration fields). Galerkin projection of the original PDE on these empirical eigenfunctions

$$v \approx \sum_{i=1}^{m} a_i(t)\phi(z), \quad w \approx \sum_{i=1}^{m} b_i(t)\psi(z) \tag{4}$$

results in a dynamical system for the time evolution of the state variable $x = [a; b]$

$$\dot{x}F(x, u) \tag{5}$$

where a and b are vectors of (POD) modal coefficients for the two concentration fields. In previous work we assumed that the full state x was accessible to measurement and thus available for feedback. Current developments in spatially resolved sensing techniques (e.g. microscopies and spectroscopies, [25]) justify the assumption of essentially continuous (in space) measurements. Here we will consider the case when only a (the v field) can be measured. The output y of the system is then given by

$$y = [I_{m\times m}, 0_{m\times m}]x \equiv Cx = a. \tag{6}$$

We are going to use a low-dimensional POD–Galerkin discretization to design first an estimator of the w-profile and subsequently a controller for the original PDE (in our case, its converged discretization, the "full system"); see the schematic Fig. 1. The controller will be implemented in discrete time with sampling interval

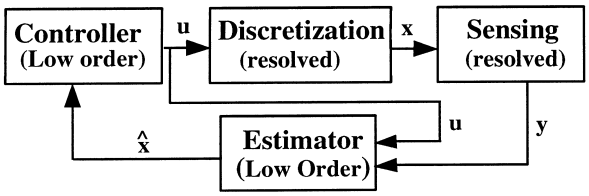

Fig. 1. Closed loop system with a low-dimensional controller. Key elements: distributed system (resolved PDE discretization or experiment), spatially resolved sensing and low dimensional controller and estimator.

$\Delta t = 2$. We convert the POD–Galerkin discretization into discrete form:

$$x_{k+1} = \Phi(x_k, u_k) \tag{7}$$

$$= x_k + \int_{k\Delta t}^{(k+1)\Delta t} (F(x(\tau)) + u_k b)\mathrm{d}\tau$$

The open loop dynamics at this nominal parameter value (see Fig. 2) exhibit a stable oscillation (a back-and-forth movement of the front location), shown in grayscale space-time plot in Fig. 2(a). The first few empirical eigenfunctions are shown in Fig. 2(b) and 2(d), while phase-space projection (on the first two eigenfunctions) of the full model attractor is compared to the same projection of the reduced model one in Fig. 2(c).

Both estimator and controller were designed based on the discrete time linear system (A_d, B_d, C)

$$e_{k+1} = A_d e_k + B_d u_k \tag{8}$$

$$y_k = C e_k \tag{9}$$

obtained (with sampling time Δt) from the linearization of the reduced order (2 POD, four degree of freedom) nonlinear model. This linearization was performed around the steady state of the reduced model ($a_1 = 0.0565$, $a_2 = -0.1476$, $b_1 = -0.0081$, $b_2 = -0.0069$) at the nominal parameter value ($\varepsilon = 0.015$).

The estimator equation (a nonlinear Luenberger observer) is obtained in a standard way from the reduced order model by adding an injection term to the vectorfield:

$$\hat{x}_{k+1} = \Phi(\hat{x}_k, u_k) + L(y_k - \hat{y}_k) \tag{10}$$

$$\hat{y}_k = C\hat{x}_k \tag{11}$$

The observer gain L was chosen to place the eigenvalues of $A_d - LC$ inside the unit circle (norm below 0.8); the tuning procedure involved testing its performance operating on a "medium size", 12-dimensional (6+6) POD–Galerkin discretization. Clearly, closed loop performance of observers and controllers based on such low-dimensional models will be affected by interaction with the

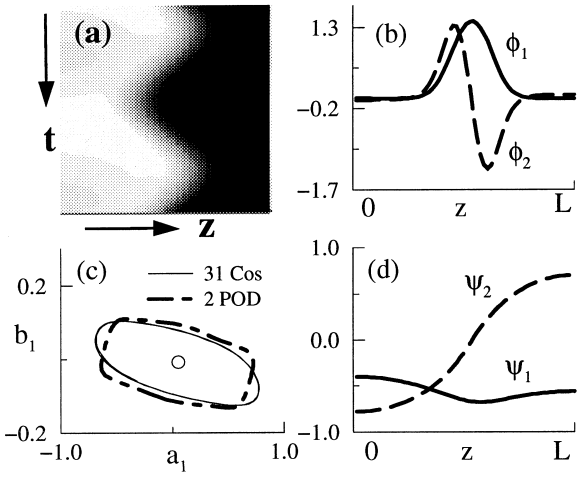

Fig. 2. Open-loop reaction–diffusion system ($\varepsilon = 0.015$): (a) space–time plot of the oscillatory front motion in arbitrary grayscale units; black (white) corresponds to high (low) levels of the v field; (b) and (d) shapes of the first two empirical eigenfunctions for v and w fields; (c) projection of the limit cycle in (a) onto the plane of the first two POD coefficients.

(unmodelled) dynamics of higher-order spatial modes. Insight in the robustness of low-dimensional design in the face of such modelling error can be gained through performance checks with a hierarchy of increasing (but still comparatively low) dimension models (see [26] for theoretical analysis of such a procedure for spectral systems).

In our particular example we designed a discrete-time Linear Quadratic Regulator minimizing the objective functional

$$J = \frac{1}{2}\sum_{i=1}^{\infty} e_k' Q e_k + u_k R u_k \tag{12}$$

The selection of the (positive definite) weighting matrices Q and R was done following the rules of thumb in [27]. The gain matrix K determining the control law $u_k = -Ke_k$ is given by

$$K = \left[B_d' S B_d + R^{-1}\right] B_d' S A_d \tag{13}$$

where S is the (positive definite) solution of the algebraic Riccati equation

$$S = A_d'\left(S - SB_d\left[B_d' S B_d + R\right]^{-1} B_d' S\right) A_d + Q \tag{14}$$

Fig. 3 shows the performance (along the full-system open-loop stable limit cycle) of the low-order model based observer; the observer is clearly capable of tracking (from a wide range of initial conditions) the state variables. This should be contrasted to the (also shown) performance of the straight *open-loop* reduced model; clearly it is not as accurate in capturing either the period or the shape of the *full system* limit cycle [a preview of

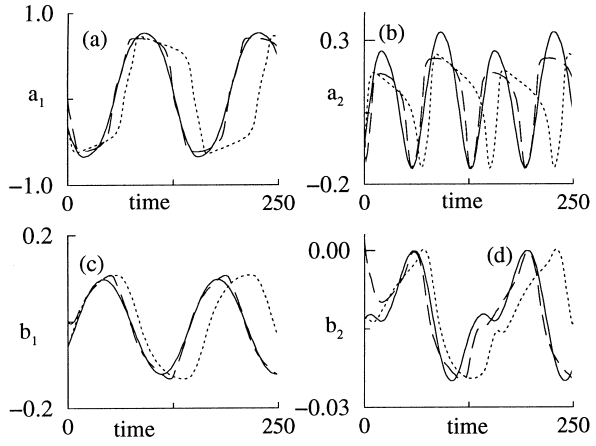

Fig. 3. Low-dimensional observer. Time series of the first two POD components for both fields along the spatiotemporal limit cycle. Solid line: resolved discretization; dashed line: "flat" two-mode POD–Galerkin truncation; long-dash line: Luenberger observer designed on the basis of the "flat" 2-mode (4 degree of freedom) truncation.

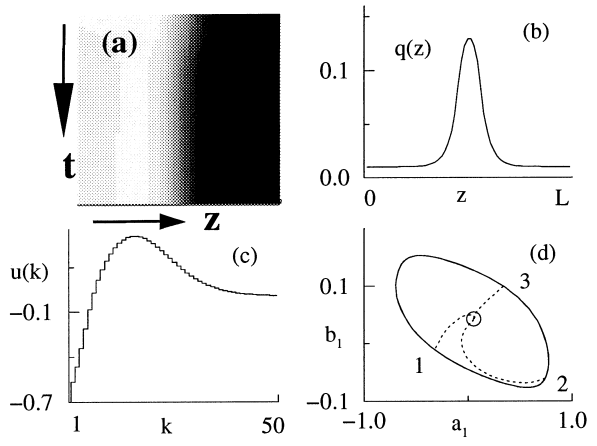

Fig. 4. Closed-loop reaction–diffusion system: (a) space–time plot of the transient leading to the stabilized set-point; (b) shape of the actuator influence function; (c) time-history of the (discrete-time) control action; (d) phase-plane projections of closed-loop transients from initial conditions (points 1, 2, 3) on the open-loop limit cycle leading to the set-point.

this was contained in Fig. 2(b)]. Fig. 4 shows the successful stabilization of the system's unstable steady state based on the controller/observer pair described above; any initial condition on the open-loop stable limit cycle surrounding the unstable steady state gives rise to closed-loop transients attracted to the set point. Higher accuracy (and better observer performance) can be obtained using successively higher order POD models. These become increasingly more complicated to evaluate in real time, and time-scale separation methods become useful in accurately reducing them. As we discussed in the introduction, black-box neural net-based models can also be efficient in further reducing "flat" POD-based Galerkin models, and in yielding easy to evaluate vectorfields for real-time applications. Here we used such an ANN to effectively "slave" the dynamics of POD modes 3, 4, 5, 6 and 7 for each field to the first two pairs of modes, thus reducing a 14-dimensional (7+7 POD mode) dynamical system to a 4-dimensional one.

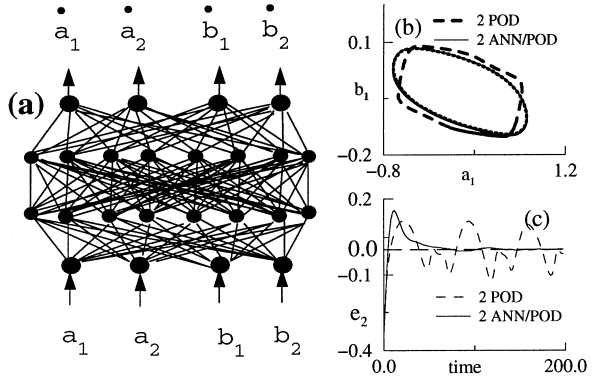

Fig. 5. (a) Architecture of the ANN used to slave higher POD mode components; (b) long-term prediction capabilities of the four ANN-fitted ODEs based on time series of the first two POD modal coefficients; (c) performance of the observer based on the ANN/POD vectorfield.

The ANN we used [see Fig. 5(a)] is a standard four-layer feed-forward neural network with four neurons in the input layer (the amplitudes of the first two POD modes for each field), and four neurons in the output layer that are trained to predict, upon convergence, the time derivatives of the four amplitudes. There are eight neurons in each of the two hidden layers (nonlinear, with sigmoidal activation function). Training is achieved using back-propagation and a conjugate gradient (CG) algorithm. The training set consisted of 500 training examples taken from transients starting close to the unstable fixed point and evolving towards the stable limit cycle. Convergence was declared after 60 complete CG iterations. We used standard cross-validation techniques to prevent over-training. This four dimensional model does a much better job in approximating the open-loop attractors [see Fig. 5(b)] than the 2-POD based one, and the (excellent) performance of the corresponding observer on the full system limit cycle is shown in Fig. 5(c) (in contrast with the 2-POD based observer); the figure shows $e_2 \equiv \hat{a}_2(t) - a_2(t)$.

2.2. Transport in a MOVPE reactor

Metal–Organic Vapor Phase Epitaxy (MOVPE) is the most versatile and cost-effective technique for growing thin films of compound semiconductors [28]. During MOVPE, vapors of organometallic compounds containing the chemical elements of the film to be deposited are diluted in a carrier gas (e.g. H_2, He, Ar, etc.) and flow over a heated substrate, resulting in the deposition of a single-crystalline film on the surface of the substrate. Multi-layer structures of such materials, called

heterostructures, form the basis of advanced electronic and opto-electronic devices. For example, quantum-well lasers emitting in the red/IR part of the spectrum consist of alternating layers of GaAs and AlAs.

To grow heterostructures by MOVPE, reactants are switched on and off periodically into a steady flow of the carrier gas. The resulting transient behavior in the reactant supply to the substrate controls the interface abruptness in the film. To form heterostructures with abrupt interfaces, transients must ideally last less than the time needed to grow one atomic layer [29]. Increasing the flow rate of the carrier gas leads to shorter transients, but also minimizes the conversion of the expensive precursors into film. Optimization of such operations requires the ability to monitor and control film quality across large substrates in real time.

A recently developed technique based on spectral reflectance [30] can be used for on line monitoring of MOVPE processes and for developing control strategies. To exploit model-based control techniques, the ability to predict the spatiotemporal behavior of the process in a real time frame is required. Thus, there is a clear need for developing *reduced order* process models that can accurately capture the spatiotemporal behavior of MOVPE.

In this work, 2-D simulations are performed to obtain the dynamics of the limiting reactant concentration profiles in a MOVPE reactor during growth of GaAs/AlAs structures from trimethyl-gallium (TMG), trimethyl-aluminum and an excess of arsine [29]. The POD method is applied to the resulting data. The most energetic (global) empirical eigenfunctions are subsequently used as a basis in the POD–Galerkin method leading to an accurate low-dimensional model capturing the relevant spatiotemporal dynamics.

The MOVPE reactor is a horizontal quartz duct with rectangular cross-section and differentially heated lower wall [29]. The heated susceptor where the substrate is placed has a uniform temperature $T_s = 950$ K. The upper wall is water cooled (300 K) and the operating pressure is 1 atm. The case of an inlet velocity $v_0 = 7.5$ cm/s which leads to a transitional flow with one small upstream recirculation near the top wall [Fig. 6(a)] is studied here, since it is near the recirculation-free limit beyond which MOVPE reactors should be operated when multilayer structures are grown [31]. Due to the high dilution of reactants in the carrier gas (H_2) the flow and heat transfer problem can be decoupled from the mass transfer and solved at steady state to obtain velocity and temperature profiles of H_2. These results are subsequently used for the solution of the dynamic mass transport model of the film precursors.

The 2-D steady state flow and heat transfer model was based on fundamental equations of continuity, momentum and energy balances [31]. The Galerkin Finite Element (FEM) technique was used to discretize the equations on a mesh consisting of 16×85 quadrilateral elements. The mesh was denser near the reactor inlet to capture steep gradients. Predicted pathlines of H_2 and the corresponding temperature profile are shown in Fig. 6(a) and (b).

To obtain instantaneous concentration profiles of TMG, 2-D dynamic simulations of the precursor's transport during steady flow of the carrier gas were performed. Reactor filling, with the precursor switched on at $t = 0$, is presented here. The precursor transport model was developed using fundamental equations for mass transfer by convection, diffusion and thermal diffusion. The mass balance for the precursor (TMG) yields:

$$\frac{\partial}{\partial t}(cx) + \nabla\cdot(cx\underline{v}) = \nabla\cdot[cD(\nabla x + k_T \nabla \ln T)] \tag{15}$$

In the above equation x is the mole fraction of the precursor, v the velocity of the gas and c the total concentration obtained at every node from the gas temperature T and pressure P using the ideal-gas law, $c = P/RT$, R being the ideal gas constant. The binary and thermal diffusion coefficients of the precursor in the carrier gas are D and k_T, respectively. The mole fraction of the carrier gas, x_N, is obtained by an overall mass balance: $x_N = 1 - x$. The boundary conditions are constant precursor mole fraction $x = x_0$ at the inlet, impermeable walls, and a natural boundary condition at the outlet. The initial condition is $x = x_0$ at the inlet and $x = 0$ everywhere else in the reactor.

The same FEM mesh as in the flow and heat transfer problem was used for the mass transfer simulations. The solution was advanced in time via an implicit Euler scheme. A small time step of 0.05 s was used to capture the initial shock from the introduction of the precursor and 200 steps were taken until the reactor almost reached steady state. Three snapshots of the TMG mole fraction profile (x-TMG) are shown in Fig. 6(i) (c), (d) and (e) at 1, 2, and 4 s, respectively. At $t = 4$ s the highest TMG concentration is not at the inlet but rather near the water-cooled top wall due to thermal diffusion [32]. Singular value decomposition of the snapshot matrix shows that the first seven modes capture 99.98% of the energy. The spatial structure of the four most energetic modes ϕ_i is shown in Fig. 6(f). The eigenmodes capture well the shape of the advancing concentration front. A POD-based Galerkin projection of the dynamic model [Eq. (15)] on the seven eigenmodes was also developed. The Galerkin projection resulted in a (low-dimensional) system of seven linear ODEs. The evolution of the amplitudes of the $\hat{\alpha}_i(t)$ coefficients obtained from the seven equation model, are shown in Fig. 7 (dashed lines). The agreement with coefficients $\hat{\alpha}_i(t)$, obtained from the projection of x-TMG from the FEM simulations on the eigenmodes (solid lines), is excellent. The reconstruction of the snapshots from the reduced model at 1, 2 and 4 s is depicted in Fig. 6(ii) (c), (d) and

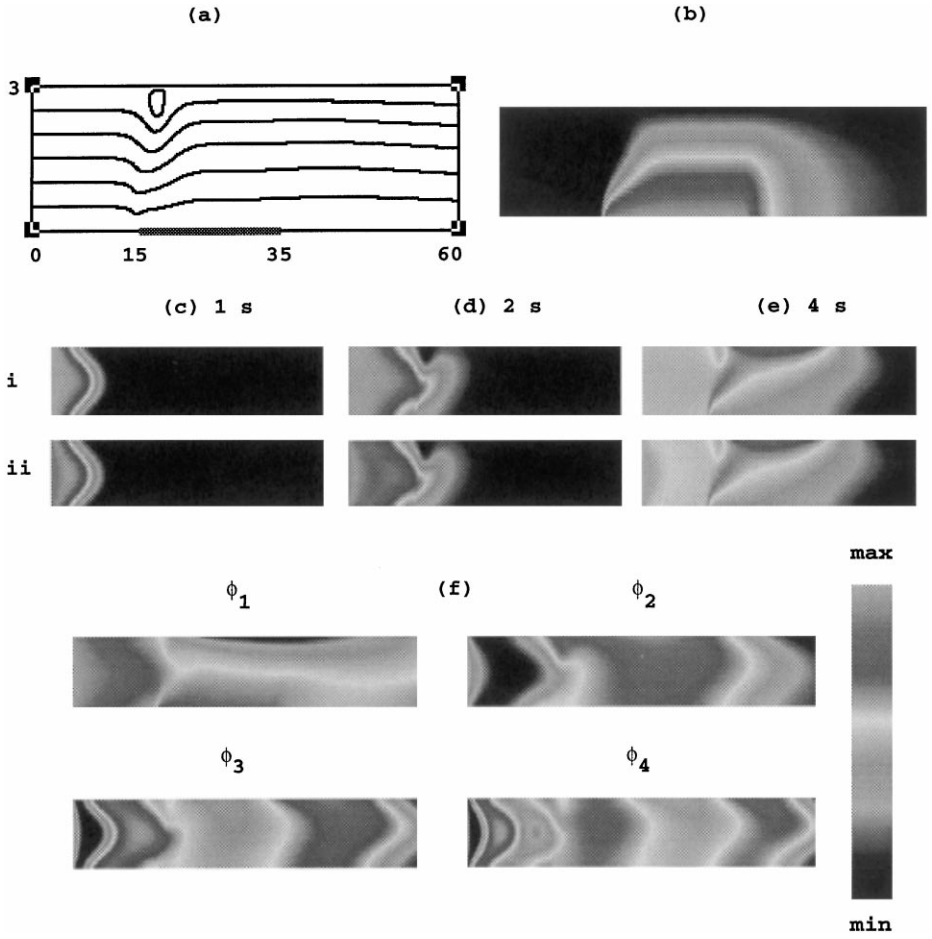

Fig. 6. MOVPE reactor model: (a) pathlines of H_2 ($v_0 = 7.5$ cm/s) (reactor dimensions are in cm); (b) temperature profile, $T_s = 950$ K; (c)–(e) (i): snapshots of x-TMG concentration from the FEM model at $t = 1$ s (c), 2 s (d), and 4 s (e); (ii) snapshots of x-TMG concentration at the same times predicted by the 7 mode Galerkin projection on empirical modes; (f) spatial structure of the four most energetic POD modes.

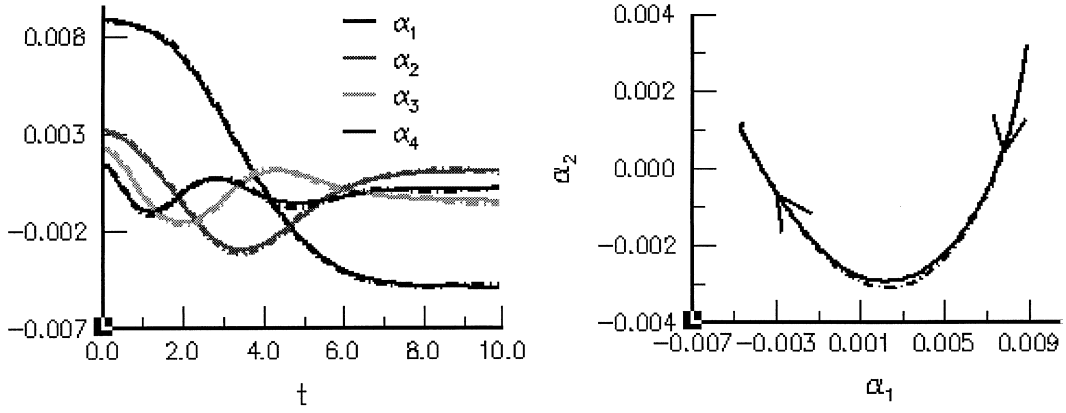

Fig. 7. (a) Time series comparison of the amplitudes of the projection of x-TMG from the FEM simulation on the four most energetic eigenmodes (solid lines) and the first four modes from the seven equation ODE model (dashed lines); (b) phase space projections of the full FEM simulation (solid line) and the reduced ODE model (dashed line).

(e), respectively. As can be seen by the comparison to the FEM data, the low dimensional ODE model can accurately predict the spatiotemporal behavior of the system and thus can successfully represent the corresponding FEM simulations. A phase-space projection of the reduced model is shown in Fig. 7(b) (dashed line) and is almost indistinguishable from the full-model projection (solid line).

The applicability of POD-based model reduction was also demonstrated for cases of different inlet flow rates (leading to flows with and without recirculations) and detailed results are to appear elsewhere [33].

3. Summary

Model order reduction techniques can be effectively used in the extraction of low-dimensional, control-relevant dynamic models of distributed reacting processes with nontrivial dynamics and/or in complex geometries. Reduced-order models possess a number of attractive properties, such as the incorporation of explicit parametric/control dependence, good use of the fundamental conservation equations, better conditioning and appropriateness for real-time use. Although reduction methods are systematic and often successful, theory does not provide practical a priori guarantees of the sizes of accurate reduced models; issues of model validation, ensemble construction, etc., are an important, and largely "experimental", part of the task. In particular, controller design based on reduced models (truncations, approximate inertial manifolds, projections on "smart" basis functions) calls for a careful analysis of the effects of modeling error. While in the case of linear systems reduced order design (at least in the case of full-state feedback) has been shown to be sufficient for closed-loop stability, the effects of model reduction induced error have not been explored systematically for nonlinear systems; a priori estimates based on functional inequalities simply do not yield practical results. The accuracy of reduced nonlinear models is thus usually tested through comparing open-loop transients. However, small open-loop errors (estimated, e.g. from comparison of specific trajectories, steady states, their spectra, etc.) may be amplified under the closed-loop conditions. Such control spillover effects were recently shown to lead to bifurcations of the closed-loop systems [9]. It is important to explore how such errors can be accounted for in the framework of conventional robust design techniques [17,34].

The main focus of this paper was to outline paths from PDE-based models to vectorfields amenable to incorporation into existing control methodologies. While theories of approximate inertial manifolds can form a rigorous basis for reduction procedures even in closed loop, the assessment of the actual size of the resulting vectorfields and the performance of controllers based on them can be obtained practically only through computer-assisted studies. The experimental demonstration of reduced model performance under closed-loop conditions for real processes, such as semiconductor manufacturing units or fluid flow systems, constitutes an important research direction and is currently underway in a number of laboratories.

Acknowledgements

This work was partially supported by NSF (SYS, EST, IGK), ARPA/ONR and UTRC (SYS, IGK). One of the authors (RRM) was supported by an Alexander von Humboldt Foundation Fellowship, and wishes to thank Professor Dr. G. Ertl and the FHI in Berlin for their hospitality. During this work EST was the Orson Anderson Scholar at the Institute of Geophysics and Planetary Physics (IGPP) at the Los Alamos National Laboratory. The work of TJM and CT has been supported by the National Science Foundation (CTS-9622204) and by the Pittsburgh Supercomputing Center.

References

[1] M.J. Balas, Toward a more practical control theory for distributed parameter systems, Control and Dynamic Systems (1982) 361–420.
[2] M.A. Balas, Nonlinear finite-dimensional control of a class of nonlinear distributed parameter systems using residual-mode filters: a proof of local exponential stability, JMAA 162 (1991) 63–70.
[3] F.J. Doyle III, H.M. Budman, M. Morari, 'Linearizing' controller design for a packed-bed reactor using a low-order wave propagation model, Ind. Eng. Chem. Res. 35 (1996) 3567–3580.
[4] P. Holmes, J.L. Lumley, G. Berkooz, Turbulence, coherent structures, dynamical systems and symmetry, Cambridge University Press, 1996.
[5] H. Aling, S. Banerjee, A.K. Bangia, V. Cole, J.L. Ebert, A. Emami-Naeini, K.F. Jensen, I.G. Kevrekidis, S. Shvartsman, Nonlinear Model Reduction for Simulation and Control of Rapid Thermal Processing, Proc. 1997 Amer. Control Conf., pp. 2923–2928.
[6] A. Theodoropoulou, R.A. Adomaitis, E.R. Zafiriou, Model reduction for optimization of rapid thermal chemical vapor deposition systems, IEEE Trans. Semic. Manuf. 11 (1) (1998) 85–98.
[7] C.C. Chen, E.-C. Chang, Accelerated disturbance damping of an unknown distributed system by nonlinear feedback, AIChE Journal 38 (9) (1992) 1461–1476.
[8] S.Y. Shvartsman, I.G. Kevrekidis, Low-dimensional approximation and control of periodic solutions in spatially extended systems, Phys. Rev. E 58 (1) (1998) 361–368.
[9] S.Y. Shvartsman, I.G. Kevrekidis, Nonlinear model reduction for control of distributed systems: a computer-assisted study, AIChE Journal 44 (7) (1998) 1579–1595.
[10] C. Foias, G.R. Sell, R. Témam, Inertial manifolds for nonlinear evolutionary equations, J. Diff. Equs. 73 (1988) 309–353.
[11] P.V. Kokotovic, H.K. Khalil, J. O'Reilly, Singular Perturbation Methods in Control: Analysis and Design, Academic Press, 1986.
[12] J. Guckenheimer, P. Holmes, Nonlinear oscillations, dynamical systems and bifurcations of vectorfields, Springer–Verlag, New York, 1983.
[13] P. Brunovsky, Controlling the dynamics of scalar reaction diffusion equations by finite dimensional controllers, in: A. Kurzhanski, I. Lasiecka (Eds), Modeling and Inverse problems of control for distributed parameter systems, 1991.
[14] H. Sano, N. Kunimatsu, Feedback control of semilinear diffusion systems: inertial manifolds for closed-loop systems, IMA J. Math. Cont. Inf. 11 (1994) 75–92.
[15] N. Kunimatsu, H. Sano, Compensator design of semilinear-parabolic systems, Int. J. Control 60 (2) (1994) 243–263.

[16] P.D. Christofides, P. Daoutidis, Finite-dimensional control of parabolic PDE systems using approximate inertial manifolds, JMAA 216 (2) (1997) 398–420.
[17] P.D. Christophides, Robust control of parabolic PDE systems, Chem. Eng. Sci. 53 (16) (1998) 2949–2965.
[18] S. Banerjee, J.V. Cole, K.F. Jensen, Designing reduced-order models for rapid thermal processing systems, J. Electrochem. Soc. 145 (11) (1998) 3974–3981.
[19] L. Sirovich, W.B. Knight, J.D. Rodriguez, Optimal low-dimensional dynamical approximations, Quart. Appl. Math. 3 (1990) 535–548.
[20] A.K. Bangia, P.F. Batcho, I.G. Kevrekidis, G.Em. Karniadakis, Unsteady 2-D flows in complex geometries: comparative bifurcation studies with global eigenfunction expansions, SIAM J. Sci. Comput. 18 (3) (1997) 775–805.
[21] K. Krischer, R. Rico-Martinez, I.G. Kevrekidis, H.H. Ertl, G. Ertl, J.L. Hudson, Model identification of a spatio-temporally varying catalytic reaction, AIChE J. 39 (1993) 89–98.
[22] C. Foias, M.S. Jolly, I.G. Kevrekidis, G.R. Sell, E.S. Titi, On the computation of inertial manifolds, Phys. Lett. A 131 (7,8) (1988) 433–436.
[23] D. Jones, E.S. Titi, A remark on quasi-stationary approximate inertial manifolds for the Navier–Stokes equations, SIAM J. Math. Anal. 25 (1994) 894–914.
[24] C. Foias, G.R. Sell, E.S. Titi, Exponential tracking and approximation of inertial manifolds for dissipative nonlinear equations, J. Dyn. Diff. Eq. 1 (1989) 199–254.
[25] H.-H. Rotermund, K. Krisher, B. Pettinger, Imaging of reaction fronts at surfaces, in: J. Lipkowski, P.N. Ross (Eds.), Frontiers of Electrochemistry. Vol. IV: Imaging of Surfaces and Interfaces, VCH Publishers, 1997.
[26] M.A. Erickson, A.J. Laub, An algorithmic test for checking stability of feedback spectral systems, Automatica 31 (1) (1995) 125–135.
[27] B.D. Moore, J.B. Anderson, Optimal Control — Linear Quadratic Methods, Prentice Hall, Englewood Cliffs, NJ, 1990.
[28] T.F. Kuech, Recent advances in metal–organic vapor phase epitaxy, Proc. IEEE 80 (1992) 1609–1624.
[29] C. Theodoropoulos, N.K. Ingle, T.J. Mountziaris, Computational studies of the transient behavior of horizontal MOVPE reactors, J. Crystal Growth 170 (1997) 72–76.
[30] W.G. Breiland, K.P. Killeen, A virtual interface method for extracting growth rates and high temperature optical constants from thin semiconductor films using in situ normal incidence reflectance, J. Appl. Phys. 78 (1995) 6726–6736.
[31] N.K. Ingle, T.J. Mountziaris, The onset of transverse recirculations during flow of gases in horizontal ducts with differentially heated lower walls, J. Fluid Mech. 277 (1994) 249–269.
[32] T.J. Mountziaris, S. Kalyanasundaram, N.K. Ingle, A reaction-transport model of GaAs growth by metalorganic chemical vapor deposition using trimethyl-gallium and tertiary-butyl arsine, J. Crystal Growth 131 (1993) 283–299.
[33] C. Theodoropoulos, T.J. Mountziaris, I.G. Kevrekidis, Order reduction of dynamic models of MOVPE, in preparation.
[34] L. Cortelezzi, J.L. Speyer, Robust reduced-order controller of laminar boundary layer transitions, Phys. Rev. E 8 (2) (1998) 1906–1910.